Structure of a left-handed DNA G-quadruplex

Wan Jun Chung, Heddi Brahim, Emmanuelle Schmitt, Kah Wai Lim, Yves Mechulam, Anh Tuân Phan

Structure of a left-handed DNA G-quadruplex

Wan Jun Chung[a], Brahim Heddi[a], Emmanuelle Schmitt[b], Kah Wai Lim[a], Yves Mechulam[b], and Anh Tuân Phan[a,1]

[a]School of Physical and Mathematical Sciences, Nanyang Technological University, Singapore 637371, Singapore; and [b]Laboratoire de Biochimie, UMR 7654, CNRS, Ecole Polytechnique, Palaiseau 91128, France

Edited by Stephen Neidle, University College London, London, United Kingdom, and accepted by the Editorial Board January 19, 2015 (received for review September 29, 2014)

Aside from the well-known double helix, DNA can also adopt an alternative four-stranded structure known as G-quadruplex. Implications of such a structure in cellular processes, as well as its therapeutic and diagnostic applications, have been reported. The G-quadruplex structure is highly polymorphic, but so far, only right-handed helical forms have been observed. Here we present the NMR solution and X-ray crystal structures of a left-handed DNA G-quadruplex. The structure displays unprecedented features that can be exploited as unique recognition elements.

G-quadruplex | left-handed helix | nucleic acid | NMR | X-ray crystallography

DNA can adopt diverse structural conformations (1–9), ranging from double helical A-, B-, and Z-forms to triplexes, quadruplexes, and branched architectures. Different DNA conformations have been associated with different biological functions (1, 2, 6, 7, 9). While the canonical double helix (1) (B-DNA) and most other structural forms follow a right-handed helical twist, Z-DNA is the only left-handed form of DNA (2) known to date.

Recent mounting biological interest has driven attention to G-quadruplex (G4) (10–16), a four-stranded structure consisting of a stack of G-tetrad layers, each comprising four guanines Hoogsteen hydrogen-bonded in a coplanar arrangement (17). This helical structure with different possible orientations between the four strands is highly polymorphic (6, 7, 16, 18, 19), but so far, only right-handed forms have been observed. G4-forming sequences are found in numerous regions of the human genome (16). Recent studies demonstrated their existence in human cells (15) and their involvement in cellular regulation including recombination (12), replication (13, 14), transcription (10), and translation (11). On the other hand, synthetic G4s have been introduced as unique structural elements in nanotechnology (20) as well as aptamers for therapeutic and diagnostic purposes (21). For instance, the G-rich oligonucleotide *AGRO100* (*SI Appendix*, Table S1), also known as *AS1411*, has been shown to exhibit potent antiproliferative activity against a range of cancer cells (21) and was later found to adopt multiple G4 conformations (22).

Herein we present NMR and X-ray structures of a G4 derived from *AGRO100*, adopted by the sequence d[T(GGT)$_4$TG(TGG)$_3$TGTT] (henceforth denoted as *Z-G4*), which exhibits distinct circular dichroism (CD) profile with a negative peak at ∼275 nm and a positive peak at ∼250 nm (Fig. 1*B*), nearly inverted from that of the right-handed G4 topologies reported to date (23). The unprecedented left-handed helical twist of *Z-G4*, as presented below, explains its atypical CD signals.

Results and Discussion

The imino proton NMR spectrum of *Z-G4* in solution containing ∼100 mM K^+ showed 16 major sharp peaks between 10.6 and 11.8 ppm (Fig. 1*A*), indicative of the formation of a four-layered G4. The NMR solution structure of *Z-G4* was elucidated (Table 1 and Fig. 2*A*) based on rigorous assignment approaches using site-specific isotopic labels and through-bond correlation experiments (*SI Appendix*, Table S2 and Figs. S1 and S2), largely following protocols described previously (18). The structure involves two continuous stacked G4 blocks (Fig. 2*D*), each comprising two G-tetrad layers arranged in the same hydrogen-bond directionalities (G2·G5·G8·G11 and G3·G6·G9·G12 for the top G4 block and G15·G18·G21·G24 and G17·G20·G23·G26 for the bottom G4 block) (*SI Appendix*, Fig. S3), connected through a central linker (T13–T14). All guanine residues adopt the *anti* glycosidic conformation with the exception of G2, which is in the *syn* conformation.

Z-G4 was successfully crystallized in the presence of potassium ions, using methylpentanediol as precipitating agent. Crystals belonged to the P3$_2$21 group and diffracted to 1.5-Å resolution. The structure was solved by molecular replacement, using the NMR solution structure as a starting model, and refined to 1.5-Å resolution (*R*-factor = 14.1%; R_{free} = 18%; Table 2 and Fig. 2*B*). Head-to-head and tail-to-tail crystal packing was observed, facilitated by thymine residues from the loops. Because of the head-to-head arrangement, two symmetry-related potassium ions are sandwiched between the two DNA molecules (*SI Appendix*, Fig. S4*A*). A hexacoordinated Mg^{2+} ion is also involved in crystal packing (*SI Appendix*, Fig. S4*B*). Similar to typical right-handed G4s, three potassium ions are visible in the core, sandwiched between the G-tetrads. Finally, 94 ordered water molecules are located mainly within the grooves and along the phosphate backbone of *Z-G4*. Electron densities, attributed to water molecules, were observed at the 5′- and 3′-ends of the G-tetrad core (Fig. 2*B*). However, the possibility of ions with low occupancy could not be excluded. Comparison between the NMR solution and X-ray crystal structures of *Z-G4* showed a high degree of concordance [pairwise rmsd of (1.63 ± 0.34) Å, excluding the last two residues] (*SI Appendix*, Fig. S5).

The strand arrangement of *Z-G4* conforms to that of a parallel-stranded G-tetrad core (Fig. 2*C*), with the average stacking distance between successive G-tetrads being (3.46 ± 0.07) Å. Dimension of all four grooves (as defined by phosphate-to-phosphate

Significance

DNA can adopt diverse structural conformations including duplexes, triplexes, and quadruplexes. Four-stranded structures known as G-quadruplexes have been implicated in cellular processes and found potential applications in therapeutics and nanotechnology. G-quadruplex structures are highly polymorphic, but so far, only right-handed helical forms have been observed. Here we present the NMR solution and X-ray crystal structures of an unprecedented left-handed DNA G-quadruplex, containing structural features that can be exploited as unique recognition elements.

Author contributions: A.T.P. initiated the project; W.J.C., B.H., and A.T.P. designed research; W.J.C., B.H., E.S., and Y.M. performed research; W.J.C., B.H., E.S., K.W.L., Y.M., and A.T.P. analyzed data; and W.J.C., B.H., E.S., K.W.L., Y.M., and A.T.P. wrote the paper.

The authors declare no conflict of interest.

This article is a PNAS Direct Submission. S.N. is a guest editor invited by the Editorial Board.

Data deposition: Atomic coordinates of *Z-G4* have been deposited in the Protein Data Bank, www.pdb.org [PDB accession codes 2MS9 (NMR solution structure) and 4U5M (X-ray crystal structure)].

[1]To whom correspondence should be addressed. Email: phantuan@ntu.edu.sg.

This article contains supporting information online at www.pnas.org/lookup/suppl/doi:10.1073/pnas.1418718112/-/DCSupplemental.

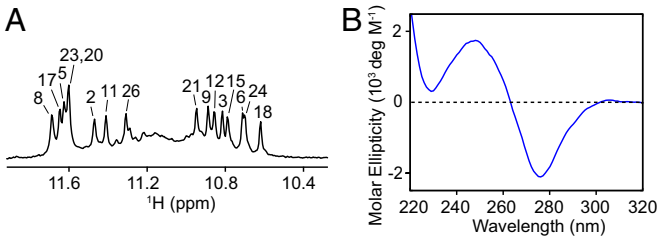

Fig. 1. (*A*) One-dimensional imino proton NMR spectrum of *Z-G4*. (*B*) CD spectrum of *Z-G4*.

distance between adjacent tetrad guanine residues) for the two G4 blocks is of medium width (~16.5 Å). The two G4 blocks are stacked through the G3·G6·G9·G12 and G15·G18·G21·G24 tetrads, consistent with the slower rate of solvent exchange of the imino protons in these tetrads as observed by NMR (*SI Appendix*, Fig. S6). Across the stacking interface, there is partial overlap between the five- and six-membered rings of the guanine bases from the two tetrad layers (between G3/G24, G12/G15, G9/G18, and G6/G21) (*SI Appendix*, Fig. S7*A*). Such stacking arrangements have previously been observed across various stacked G4 structures (24) (*SI Appendix*, Fig. S7*B*). However, as opposed to that observed in right-handed G4 structures, O4′ atoms of the sugar residues in *Z-G4* point in the direction of the strand progression (*SI Appendix*, Fig. S8 *A* and *B*).

Within each G4 block, strands are connected by single-nucleotide thymine loops (T4, T7, and T10 for the top G4 block and T16, T19, T22, and T25 for the bottom G4 block). The backbone configuration of these loops deviates from that of a typical single-nucleotide propeller loop (25). Instead of flipping outward, thymine bases T7, T10, T13, T16, T19, T22, and T25 collapse onto the terminal G-tetrads, allowing the O4′ atoms of these residues to establish a hydrogen bond with the amino protons of the nearby tetrad guanine bases (G5, G8, G11, G26, G17, G20, and G23) (Fig. 3 and *SI Appendix*, Fig. S9 *A* and *C*). In the crystal structure, the relatively low B factors of these thymines (ranging between 13.4 and 17.2 Å^2 for T7, T10, T13, T22, and T25; 27.4 Å^2 for T16; and 22.6 Å^2 for T19), only slightly higher than the mean B-factor of guanines in the G-tetrad core (13.6 Å^2), indicated that these residues were well ordered. These structural arrangements are supported by the slow rate of solvent exchange of the guanine amino protons as observed by NMR (*SI Appendix*, Fig. S9 *B* and *C*). We also note alternative structural conformations for residues T4, G5, and T10. The accessible grooves and the capping of both G-tetrad ends by the thymines create a unique structural motif that could potentially serve as specific recognition element (Fig. 3).

All taken together, general characteristics (e.g., tetrad geometry, groove dimensions, and stacking distances) of *Z-G4* comply with those of a regular right-handed G4. However, backbone progression of successive guanine residues constituting each individual G4 block is left-handed (Fig. 4 *A* and *E*), which is reverse of that of a typical all-parallel-stranded G4 scaffold (e.g., monomeric three-layered G4 formed by the sequence d[TT(GGGT)$_4$], henceforth denoted as *T95-2T*; *SI Appendix*, Table S1, and Fig. 4 *B* and *F*) (25). Looking down each G4 block from 5′ to 3′, the oligonucleotide strand progresses in an anticlockwise manner for *Z-G4* (Fig. 4*C*), in contrast to *T95-2T*, in which the oligonucleotide strand progresses in a clockwise manner (Fig. 4*D*). On average, the relative rotation/twist between two successive guanine bases is reverse, (−25.73 ± 2.00)° for *Z-G4* vs. (+29.41 ± 2.45)° for *T95-2T* (Fig. 4 *G* and *H*). Such helical geometries are reflected by their contrasting CD spectra (*SI Appendix*, Fig. S10), which are almost mirror images of one another. Similar contrasting behavior was previously reported between Z-DNA and B-DNA (26). Analysis of the backbone dihedrals for *Z-G4* revealed a unique left turn: torsion angles for the dinucleotide steps G5–G6, G8–G9, G11–G12, G17–G18, G20–G21, and G23–G24 approximate those observed in Z-DNA for nucleotides in the *anti* conformation (which would have largely accounted for the left-handed progression of the G4 block) (Table 3 and *SI Appendix*, Fig. S11). Furthermore, a similar Z-DNA–like backbone configuration can be observed for the G2–G3 step of *Z-G4* (*SI Appendix*, Fig. S12). Such unusual local backbone conformations have recently been observed to occur in RNA quadruplex aptamers (27–29). Previously, quadruplexes

Table 1. NMR restraints and structure statistics

Restraints and structure statistics	Value
NMR restraints	
Distance restraints	
Intraresidue	
Exchangeable	3
Nonexchangeable	310
Interresidue	
Exchangeable	105
Nonexchangeable	246
Hydrogen bond restraints	64
Structure statistics	
NOE violations	
Numbers (>0.2 Å)	0.500 ± 0.671
Deviations from standard geometry	
Bond length, Å	0.005 ± 0.000
Bond angle, °	0.800 ± 0.013
Impropers, °	0.448 ± 0.024
Pairwise all heavy atom rmsd values, Å	
All heavy atoms	1.950 ± 0.250
G-tetrad core	1.089 ± 0.137

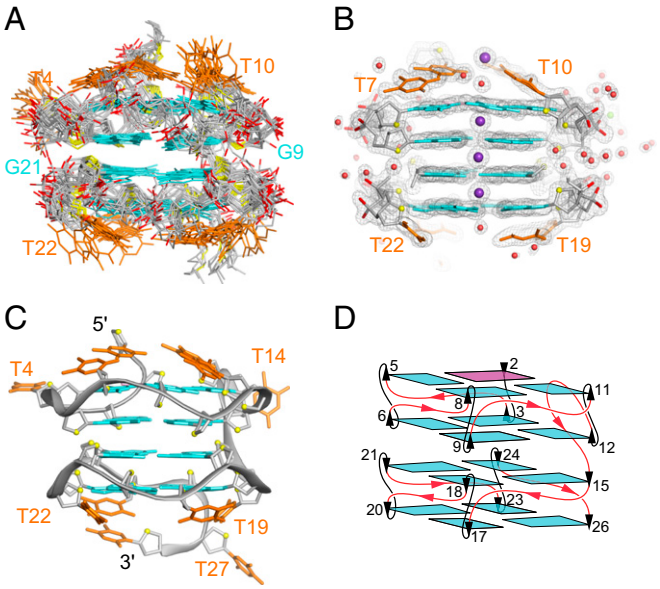

Fig. 2. (*A*) Ten lowest-energy superimposed solution structures of *Z-G4*. (*B*) Crystal structure of *Z-G4*. The electron density corresponds to the final 2mFo-DFc map contoured at 1.0 σ. (*C*) Ribbon view of the crystal structure of *Z-G4*. *Anti* and *syn* guanine bases are colored in cyan and magenta, respectively; thymine bases are in orange; phosphate backbone are in gray; phosphate oxygens are in red; and O4′ oxygens are in yellow. Potassium ions and water molecules are colored in purple and red, respectively. (*D*) Schematic structure of *Z-G4*. Arrows represent the 5′-to-3′ strand progression.

Table 2. Data collection and refinement statistics for X-ray crystal structure determination

Data collection and refinement statistics	Value
Data collection*	
Space group	$P3_221$
Cell dimensions	
a, *b*, *c*, Å	51.90, 51.90, 40.17
α, β, γ, °	90.0, 90.0, 120.0
Resolution, Å	44.9–1.5
R_{sym}	0.083 (0.642)†
I/σI	18.50 (2.76)
Completeness, %	95.7 (77.7)
Redundancy	9.2 (5.6)
Refinement	
Resolution, Å	44.9–1.5
Number of reflections	9875
R_{work}/R_{free}	0.1410/0.1800
Number of atoms	
DNA	631
K^+	4
Mg^{2+}	1
Water	94
B-factors, Å^2	
DNA	16.81
K^+	10.22
Mg^{2+}	35.63
Water	31.66
rmsd	
Bond lengths, Å	0.008
Bond angles, °	1.090

*A single crystal was used for data collection.
†Values in parentheses are for the highest-resolution shell.

with left-handed helicity have been artificially induced through full or partial incorporation of enantiomeric L-nucleotides (30, 31).

NMR and CD spectra showed that *Z-G4* adopted the same left-handed G4 scaffold under near-physiological ionic condition

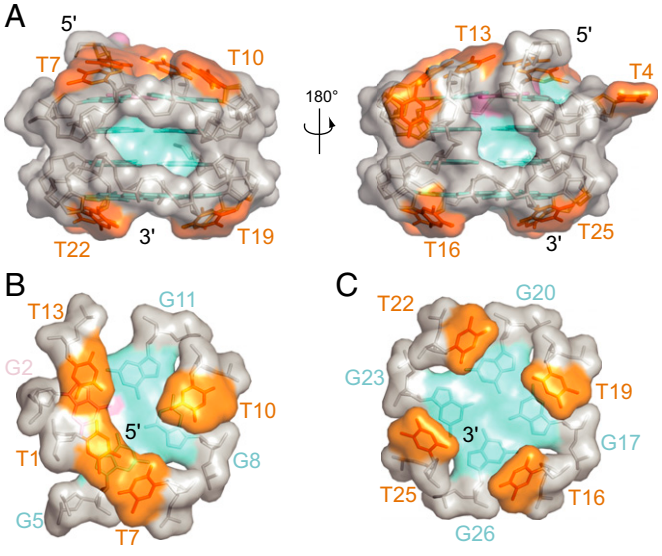

Fig. 3. Surface representation showing the capping of the top and bottom tetrad. (*A*) Side views. (*B*) Top view. (*C*) Bottom view. *Anti* and *syn* guanine bases are colored in cyan and magenta, respectively; thymine bases are in orange; phosphate backbone is colored in gray. Bases are labeled with their corresponding residue numbers.

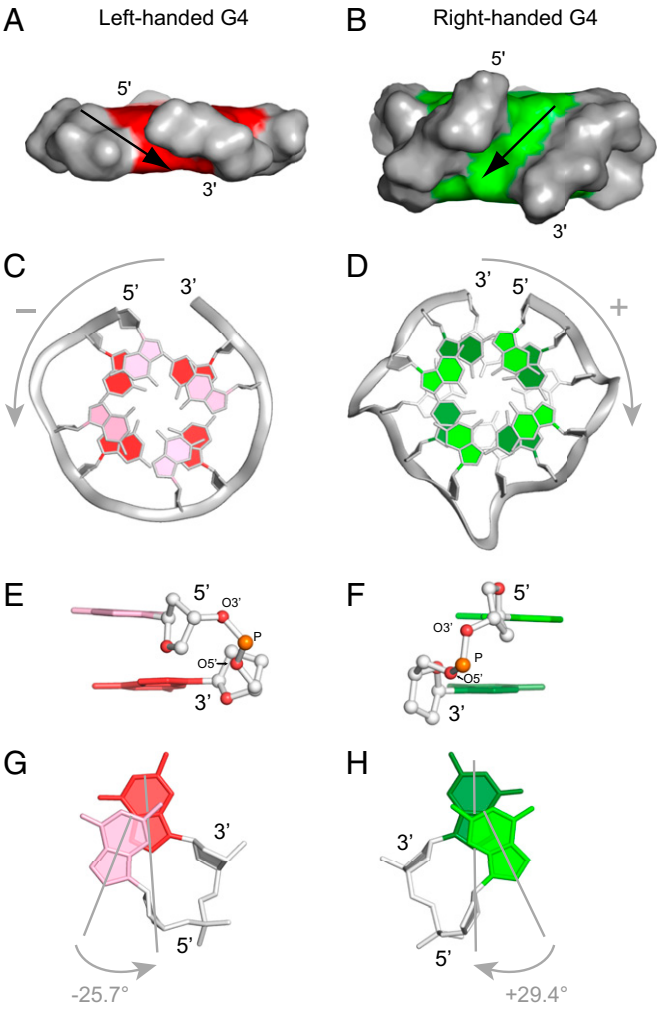

Fig. 4. (*A*) Surface representation of one block (two tetrad layers) of *Z-G4* showing the left-handed directionality of the phosphate backbone. (*B*) Surface representation of *T95-2T* (Protein Data Bank code 2LK7) (three tetrad layers) showing the right-handed directionality of the phosphate backbone. Thymine residues are removed for clarity. (*C*) Top view from the 5′ end of *Z-G4* showing the anticlockwise progression of the backbone, as depicted by the gray arrow. (*D*) Top view from the 5′ end of *T95-2T* showing the clockwise progression of the backbone, as depicted by the gray arrow. (*E*) Side view of a representative dinucleotide step of *Z-G4*. (*F*) Side view of a representative dinucleotide step of *T95-2T*. (*G*) (Top view) Stacking between two successive guanines within a subunit of *Z-G4* with a relative rotation of –25.7°. (*H*) (Top view) Stacking between two successive guanines in *T95-2T* with a relative rotation of +29.4°.

in solution containing 160 mM K^+, 10 mM Na^+, and 2 mM Mg^{2+} (*SI Appendix*, Fig. S13) but not in a Li^+-containing buffer, pointing toward the role of K^+ ions in the stabilization of the G-tetrad core. CD experiments (*SI Appendix*, Fig. S14) showed that the *Z-G4* structure was formed under different K^+ concentrations and that its thermal stability increased with increasing K^+ concentration (melting temperature, T_m ~45 °C at 90 mM K^+; T_m ~62 °C at 700 mM K^+). Sequence modifications on the central linker T13–T14 (e.g., reduction to one or zero nucleotides, or extension to four nucleotides) and on the first loop T4 (e.g., T-to-A, T-to-C, and T-to-TT) were well tolerated (*SI Appendix*, Table S3 and Fig. S15). Modifications at both ends, resulting in *AGRO100* (*SI Appendix*, Table S1), could also be tolerated, as observed from the similarity between the NMR and CD spectra of *Z-G4* and those of one isolated fraction of *AGRO100* (22).

Table 3. Comparison of backbone torsion angles of *Z-G4* with various right- and left-handed DNA forms

	Quadruplex		Duplex	
Backbone dihedral	*Z-G4**	Regular G4[†]	Z-DNA[‡] *anti–syn/syn–anti*	B-DNA[§]
ε	(316 ± 2)°	(197 ± 9)°	(267 ± 9)°/(240 ± 9)°	(184 ± 11)°
ζ	(86 ± 3)°	(250 ± 10)°	(75 ± 9)°/(301 ± 16)°	(265 ± 10)°
α+1	(161 ± 6)°	(309 ± 17)°	(71 ± 13)°/(201 ± 20)°	(298 ± 15)°
β+1	(226 ± 5)°	(180 ± 8)°	(183 ± 9)°/(225 ± 16)°	(176 ± 9)°
γ+1	(54 ± 3)°	(33 ± 11)°	(179 ± 9)°/(54 ± 13)°	(48 ± 11)°

*Average values and standard deviations as obtained from the six dinucleotide steps G5–G6, G8–G9, G11–G12, G17–G18, G20–G21, and G23–G24.

[†]Average values and standard deviations as obtained from eight dinucleotide steps G2–G3, G3–G4, G8–G9, G9–G10, G14–G15, G15-G16, G20-G21, and G21–G22 in a three-layered parallel-stranded G-quadruplex (Protein Data Bank code 1KF1) (7).

[‡]Parameters are listed for *anti–syn* and *syn–anti* steps of ZI phosphate conformation (42).

[§]BI phosphate conformation (42).

The left-handed helical nature of *Z-G4* gives rise to a unique G4 scaffold featuring several unprecedented structural motifs, which could serve as natural or artificial recognition elements. Sequence matches of *Z-G4* were found in various locations of the human genome (*SI Appendix*, Table S4), whereas results from sequence modifications suggested scope for expanding the sequence definition of such a left-handed G-quadruplex structure. These motifs could build upon the toolbox available for the construction of DNA assemblies (32). The topology of *Z-G4* reveals unprecedented folding principles of G-rich oligonucleotides that could be applied toward the design and prediction of G4 motifs. Furthermore, the compact structure of *Z-G4* could facilitate its potential application as an aptamer for therapeutic or diagnostic purposes.

Methods

Sample Preparation. The unlabeled and site-specific labeled DNA oligonucleotides were chemically synthesized on an ABI 394 DNA/RNA synthesizer. DNA sample concentrations were determined by measuring the UV absorbance at 260 nm.

Circular Dichroism. Circular dichroism (CD) spectra were recorded at 25 °C using a JASCO-815 spectropolarimeter with a 1-cm path length quartz cuvette containing a solution volume of 500 μL. Spectra (220–320 nm) were taken with a scan speed of 200 nm/min. DNA (~5 μM) was dissolved in a buffer containing 70 mM KCl and 20 mM potassium phosphate, pH 7.0. For each measurement, an average of three scans was taken, and the spectral contribution of the buffer was subtracted.

NMR Spectroscopy. Unless otherwise stated, all NMR experiments were performed on 600- and 700-MHz Bruker spectrometers at 25 °C. The concentration of DNA samples was typically 0.1–2 mM. Solution contained 70 mM KCl, 20 mM potassium phosphate (pH 7.0), and 10% (vol/vol) D_2O. Spectral analyses were performed using SpinWorks (home.cc.umanitoba.ca/~wolowiec/spinworks/), FELIX (Felix NMR, Inc.), and SPARKY (33).

NMR-Restrained Structure Calculation. Interproton distances for *Z-G4* were classified based on NOESY experiments performed in D_2O (mixing times, 100 and 300 ms) and H_2O (mixing time, 200 ms). The structure of *Z-G4* was calculated using X-PLOR-NIH (34) and AMBER (35). Detailed procedures are described in *SI Appendix*. Structures were displayed using PyMOL (36).

Crystallization and X-Ray Crystallography. Crystallization assays were performed by the sitting-drop methods, using a solution of *Z-G4* (2 mM) in 10 mM potassium cacodylate buffer (pH 6.5) and 100 mM potassium chloride. Initial screening was done with the Natrix commercial screens (Hampton Research). Hexagonal crystals (space group $P3_221$) were obtained using 35% (vol/vol) methylpentanediol as precipitating agent, in the presence of 40 mM sodium cacodylate (pH 7.0), 20 mM magnesium chloride, 12 mM potassium chloride, and 80 mM sodium chloride. For data collection, crystals were directly flash frozen in liquid nitrogen. Data were collected from a single crystal at the SOLEIL PROXIMA 1 beamline (λ = 0.979 Å; Saint-Aubin, France) equipped with a Pilatus detector and processed using XDS (37). Data collection statistics are summarized in Table 2. Initially, the structure was solved by molecular replacement, using PHASER (38) with data to 2.5-Å resolution. The coordinates of the G residues from the NMR structure were used as a search model. The model was then refined and completed with the T residues as well as ions and water molecules, by several cycles of manual building using Coot (39) and energy minimization using phenix.refine (40). In the last steps of refinement, anisotropic B-factors were used. The final model contains all 28 residues of DNA, 4 potassium ions, 1 magnesium ion, and 94 water molecules (Table 2). A representative portion of the final electron density is illustrated in *SI Appendix*, Fig. S16.

Structural Analysis. Structures were analyzed using an in-house script and Curves+ (41). The twist angle between two successive guanines was calculated as the angle between the vectors formed by the C8 atom coordinate and the middle point of the N1, C2 atom coordinates. The rise between two successive guanines was calculated as the distance between two averaged planes formed by the aromatics rings of guanine residues. Backbone dihedral angles were calculated using Curves+.

ACKNOWLEDGMENTS. We thank Ngoc Quang Do and Eugene Choon Guobin for their participation in the early stages of the project, as well as the staff of the PROXIMA 1 beamline at SOLEIL for expert assistance during data collection. This work was supported by Singapore Ministry of Education Academic Research Fund Tier 3 (MOE2012-T3-1-001) and Tier 2 (MOE2012-T2-1-102), grants from Nanyang Technological University (to A.T.P.), and grants from the Centre National de la Recherche Scientifique and Ecole Polytechnique to the UMR7654 laboratory.

1. Watson JD, Crick FHC (1953) Molecular structure of nucleic acids; a structure for deoxyribose nucleic acid. *Nature* 171(4356):737–738.
2. Wang AHJ, et al. (1979) Molecular structure of a left-handed double helical DNA fragment at atomic resolution. *Nature* 282(5740):680–686.
3. Leontis NB, Stombaugh J, Westhof E (2002) The non-Watson-Crick base pairs and their associated isostericity matrices. *Nucleic Acids Res* 30(16):3497–3531.
4. Nikolova EN, et al. (2011) Transient Hoogsteen base pairs in canonical duplex DNA. *Nature* 470(7335):498–502.
5. Frank-Kamenetskii MD, Mirkin SM (1995) Triplex DNA structures. *Annu Rev Biochem* 64:65–95.
6. Smith FW, Feigon J (1992) Quadruplex structure of *Oxytricha* telomeric DNA oligonucleotides. *Nature* 356(6365):164–168.
7. Parkinson GN, Lee MPH, Neidle S (2002) Crystal structure of parallel quadruplexes from human telomeric DNA. *Nature* 417(6891):876–880.
8. Gehring K, Leroy JL, Guéron M (1993) A tetrameric DNA structure with protonated cytosine–cytosine base pairs. *Nature* 363(6429):561–565.
9. Lilley DMJ (2000) Structures of helical junctions in nucleic acids. *Q Rev Biophys* 33(2):109–159.
10. Siddiqui-Jain A, Grand CL, Bearss DJ, Hurley LH (2002) Direct evidence for a G-quadruplex in a promoter region and its targeting with a small molecule to repress c-*MYC* transcription. *Proc Natl Acad Sci USA* 99(18):11593–11598.
11. Kumari S, Bugaut A, Huppert JL, Balasubramanian S (2007) An RNA G-quadruplex in the 5′ UTR of the NRAS proto-oncogene modulates translation. *Nat Chem Biol* 3(4):218–221.

12. Cahoon LA, Seifert HS (2009) An alternative DNA structure is necessary for pilin antigenic variation in *Neisseria gonorrhoeae*. *Science* 325(5941):764–767.
13. Paeschke K, Capra JA, Zakian VA (2011) DNA replication through G-quadruplex motifs is promoted by the *Saccharomyces cerevisiae* Pif1 DNA helicase. *Cell* 145(5):678–691.
14. Lopes J, et al. (2011) G-quadruplex-induced instability during leading-strand replication. *EMBO J* 30(19):4033–4046.
15. Biffi G, Tannahill D, McCafferty J, Balasubramanian S (2013) Quantitative visualization of DNA G-quadruplex structures in human cells. *Nat Chem* 5(3):182–186.
16. Maizels N, Gray LT (2013) The G4 genome. *PLoS Genet* 9(4):e1003468.
17. Gellert M, Lipsett MN, Davies DR (1962) Helix formation by guanylic acid. *Proc Natl Acad Sci USA* 48(12):2013–2018.
18. Adrian M, Heddi B, Phan AT (2012) NMR spectroscopy of G-quadruplexes. *Methods* 57(1):11–24.
19. Trajkovski M, da Silva MW, Plavec J (2012) Unique structural features of interconverting monomeric and dimeric G-quadruplexes adopted by a sequence from the intron of the N-myc gene. *J Am Chem Soc* 134(9):4132–4141.
20. Yatsunyk LA, Mendoza O, Mergny JL (2014) "Nano-oddities": Unusual nucleic acid assemblies for DNA-based nanostructures and nanodevices. *Acc Chem Res* 47(6):1836–1844.
21. Bates PJ, Laber DA, Miller DM, Thomas SD, Trent JO (2009) Discovery and development of the G-rich oligonucleotide AS1411 as a novel treatment for cancer. *Exp Mol Pathol* 86(3):151–164.
22. Dailey MM, Miller MC, Bates PJ, Lane AN, Trent JO (2010) Resolution and characterization of the structural polymorphism of a single quadruplex-forming sequence. *Nucleic Acids Res* 38(14):4877–4888.
23. Vorlíčková M, Kejnovská I, Bednářová K, Renčiuk D, Kypr J (2012) Circular dichroism spectroscopy of DNA: From duplexes to quadruplexes. *Chirality* 24(9):691–698.
24. Lech CJ, Heddi B, Phan AT (2013) Guanine base stacking in G-quadruplex nucleic acids. *Nucleic Acids Res* 41(3):2034–2046.
25. Do NQ, Phan AT (2012) Monomer-dimer equilibrium for the 5′-5′ stacking of propeller-type parallel-stranded G-quadruplexes: NMR structural study. *Chemistry* 18(46): 14752–14759.
26. Pohl FM, Jovin TM (1972) Salt-induced co-operative conformational change of a synthetic DNA: Equilibrium and kinetic studies with poly (dG-dC). *J Mol Biol* 67(3):375–396.
27. Phan AT, et al. (2011) Structure-function studies of FMRP RGG peptide recognition of an RNA duplex-quadruplex junction. *Nat Struct Mol Biol* 18(7):796–804.
28. Huang H, et al. (2014) A G-quadruplex-containing RNA activates fluorescence in a GFP-like fluorophore. *Nat Chem Biol* 10(8):686–691.
29. Warner KD, et al. (2014) Structural basis for activity of highly efficient RNA mimics of green fluorescent protein. *Nat Struct Mol Biol* 21(8):658–663.
30. Tran PLT, Moriyama R, Maruyama A, Rayner B, Mergny JL (2011) A mirror-image tetramolecular DNA quadruplex. *Chem Commun* 47(19):5437–5439.
31. Virgilio A, et al. (2011) Unprecedented right- and left-handed quadruplex structures formed by heterochiral oligodeoxyribonucleotides. *Biochimie* 93(7):1193–1196.
32. Seeman NC (2010) Nanomaterials based on DNA. *Annu Rev Biochem* 79:65–87.
33. Goddard TD, Kneller DG *SPARKY 3* (University of California, San Francisco).
34. Schwieters CD, Kuszewski JJ, Tjandra N, Clore GM (2003) The Xplor-NIH NMR molecular structure determination package. *J Magn Reson* 160(1):65–73.
35. Case DA, et al. (2005) The Amber biomolecular simulation programs. *J Comput Chem* 26(16):1668–1688.
36. DeLano WL, Bromberg S (2004) *PyMOL User's Guide* (DeLano Scientific LLC, San Carlos, CA).
37. Kabsch W (2010) XDS. *Acta Crystallogr D Biol Crystallogr* 66(Pt 2):125–132.
38. McCoy AJ, et al. (2007) *Phaser* crystallographic software. *J Appl Cryst* 40(Pt 4):658–674.
39. Emsley P, Lohkamp B, Scott WG, Cowtan K (2010) Features and development of *Coot*. *Acta Crystallogr D Biol Crystallogr* 66(Pt 4):486–501.
40. Afonine PV, et al. (2012) Towards automated crystallographic structure refinement with *phenix.refine*. *Acta Crystallogr D Biol Crystallogr* 68(Pt 4):352–367.
41. Lavery R, Moakher M, Maddocks JH, Petkeviciute D, Zakrzewska K (2009) Conformational analysis of nucleic acids revisited: Curves+. *Nucleic Acids Res* 37(17):5917–5929.
42. Schneider B, Neidle S, Berman HM (1997) Conformations of the sugar-phosphate backbone in helical DNA crystal structures. *Biopolymers* 42(1):113–124.